Geotextiles and Geomembranes 26 (2008) 460–472

Contents lists available at ScienceDirect

Geotextiles and Geomembranes

journal homepage: www.elsevier.com/locate/geotexmem

Performance of a two-tier geosynthetic reinforced segmental retaining wall under a surcharge load: Full-scale load test and 3D finite element analysis

Chungsik Yoo*, Sun-Bin Kim[1]

Department of Civil and Environmental Engineering, Sungkyunkwan University, 300 Chun-Chun Dong, Jan-An Gu, Suwon, Kyong-Gi Do 440-746, Republic of Korea

ARTICLE INFO

Article history:
Received 5 July 2007
Received in revised form 13 April 2008
Accepted 7 May 2008
Available online 7 July 2008

Keywords:
Reinforced soil wall
Segmental retaining wall
Tiered wall
Surcharge load
Geogrid
Bridge abutment

ABSTRACT

This paper presents the results of a full-scale load test and a 3D finite element analysis on a two-tier, 5 m high, geosynthetic reinforced segmental retaining wall (GR-SRW) subjected to a surcharge load aiming at investigating the response of the GR-SRW to various levels of surcharge load. The results of the load test at working stress condition revealed that the GR-SRW's response to the test load was well within the serviceability limits, and that the currently available design guideline tends to over-estimate the surcharge load-induced reinforcement forces. The predicted results for the surcharge load well in excess of the test load indicated that the surcharge load-induced reinforcement strains exponentially decrease with depth, showing a good agreement in qualitative terms with that assumed in the FHWA design guideline. The predicted wall deformation at the allowable bearing pressure of 200 kPa was within the serviceability level demonstrating an excellent load carrying capacity of the GR-SRW. Design implications and the findings from this study are discussed.

1. Introduction

The use and acceptance of geosynthetic reinforced segmental retaining walls (GR-SRWs) in both private and public sectors are increasing worldwide as the GR-SRWs have demonstrated several advantages such as sound performance, aesthetics, cost effectiveness, expediency of construction, good seismic performance, and the ability to tolerate large differential settlement without distress. There has been considerable recent research relating to reinforced soil walls (e.g. Al Hattamleh and Muhunthan, 2006; Nouri et al., 2006; Chen et al., 2007; Won and Kim, 2007; Chen and Chiu, 2008) and many geosynthetic reinforced soil walls have been safely constructed and are performing well to date. However, there are many areas that need in-depth studies to safely construct GR-SRW systems under more aggressive and complex boundary conditions.

Recently GR-SRWs are frequently adopted in bridge construction in public sectors, as the form of geosynthetic reinforced soil (GRS) abutments in bridge applications (Lee and Wu, 2004). One of the advantages of the GRS abutment is to alleviate the "bridge bump" caused by differential settlements between the bridge abutment and approach way. The GRS bridge-supporting structure can be constructed using either rigid or flexible facings. A "rigid" facing is either precast or cast-in-place type while a "flexible" facing takes the form of wrapped geosynthetic sheets, segmental blocks, or gabions (Lee and Wu, 2004). Lee and Wu (2004) synthesized measured data of four in-service GRS bridge abutments and six full-scale field experiments, and concluded that GRS bridge abutments with flexible facing are indeed an adequate alternative to conventional bridge abutments.

When using a GR-SRW as a load supporting structure such as the bridge abutment, it is imperative to fully understand the effect of the load on the wall performance. A few field experimental studies concerning GRS bridge-supporting structures are available up to date, including Werner and Resl (1986), Miyata and Kawasaki (1994), Benigni et al. (1996), Gotteland et al. (1997), Adams (1997), Ketchart and Wu (1997), among others. Gotteland et al. (1997) conducted a full-scale experiment to investigate the failure behavior of GRS structures as bridge abutments using a 4.35 m high GRS embankment loaded by foundation slab. Adams (1997) in particular reported the results of a full-scale bridge pier test performed at the Turner-Fairbank Highway Research Center, FHWA in McLean, Virginia, USA. They reported, among others, that the GRS pier performed satisfactorily at the allowable bearing pressure of 200 kPa, and that the preloading of the GRS pier at the top can be an effective means of reducing vertical settlement of the GRS pier. Wu et al. (2001) also reported the results of the load test on a GRS abutment, in which the effect of preloading of the GRS abutment with a preset load level at the top on the GRS abutment performance was studied. They concluded that the preloading can be an

* Corresponding author. Tel.: +82 31 290 7518; fax: +82 31 290 7549.
E-mail addresses: csyoo@skku.edu (C. Yoo), ksb9677@hanmail.net (S.-B. Kim).
[1] Tel.: +82 31 290 7537; fax: +82 31 290 7549.

0266-1144/$ – see front matter © 2008 Elsevier Ltd. All rights reserved.
doi:10.1016/j.geotexmem.2008.05.008

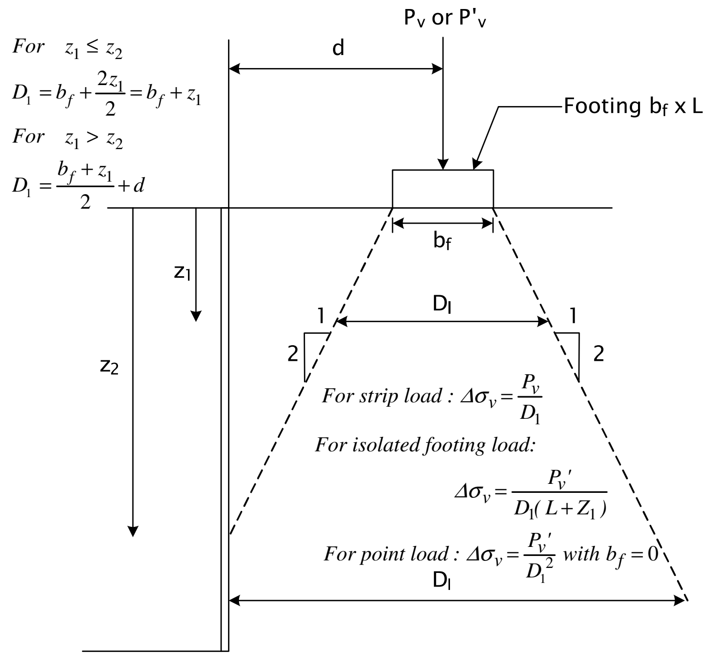

Fig. 1. 2V:1H pyramid distribution adopted in FHWA design guideline.

efficient measure in reducing a GRS abutment deformation as well as creep strain of reinforcement. Aforementioned previous studies proved that the geosynthetic reinforced soil technology may be effectively used as a viable alternative to conventional bridge-supporting structures.

There are many situations where GR-SRWs are constructed in a tiered configuration for a variety of reasons such as aesthetics, stability, and construction constraints, etc. For the bridge abutment application in particular, GR-SRWs are frequently constructed in a tiered configuration. Although there have been a number of studies concerning the GRS walls in tiered configuration (Leshchinsky and Han, 2004; Yoo and Kim, 2002; Yoo and Jung, 2004; Yoo and Song, 2006), most of them focused on the effect of offset distance between upper and lower tiers on the wall performance during construction. In addition no criteria for dealing with the effect of a surcharge load on a tiered GR-SRW are addressed in the current design guidelines such as NCMA (1997) and FHWA (2001) design guidelines. As the use of tiered GR-SRWs in bridge abutment construction is increasing, there is a definite need for an in-depth study on the response of a two-tier geosynthetic reinforced segmental retaining wall to a surcharge load, which helps to accumulate relevant data to extend or refine the current design guidelines.

In the present investigation, the results of a full-scale load test and a 3D finite element analysis on a 5 m high, two-tier GR-SRW are presented. Primary objectives of the load test were to evaluate the performance of the two-tier GR-SRW under a surcharge load at working load level and to furnish a complete set of data for calibration of the three-dimensional finite element model. The 3D finite element analysis on the other hand aimed at investigating the wall response to surcharge loads well beyond the test load level.

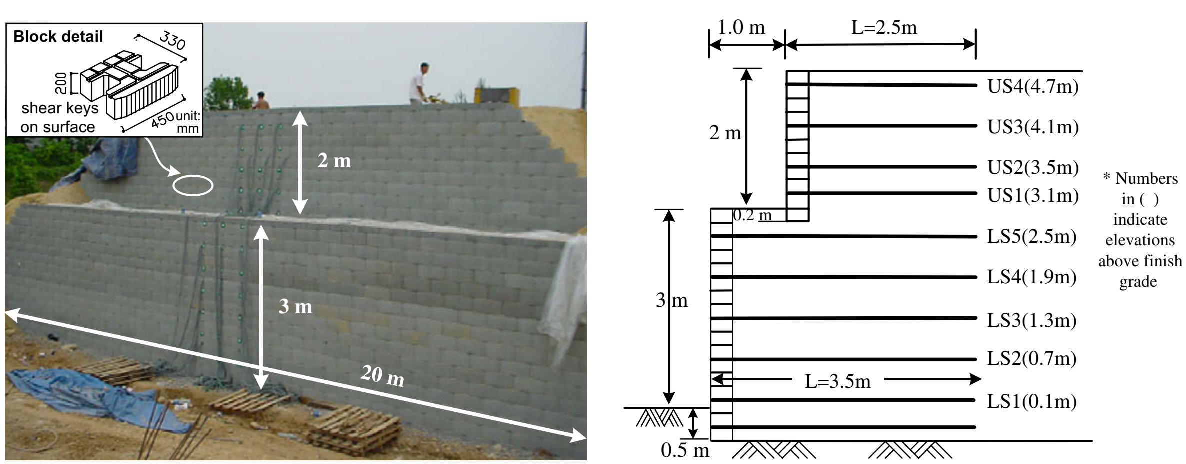

(a) photo of completed wall (b) sectional view

Fig. 2. Test wall configuration.

Fig. 3. Surcharge load using PC box.

This paper describes the test wall, the load test program including the instrumentation, details of the observed performance, and the results of the 3D finite element analysis.

2. Design consideration

In a surcharge loaded GRS or mechanically stabilized earth (MSE) wall, i.e., a GRS wall supporting a bridge beam when used as a bridge abutment, the effect of the surcharge load on the reinforced soil structure is to increase vertical stresses in the reinforced soil mass, thereby increasing the tensile forces in the reinforcement. One of the key design issues is therefore to determine the vertical stress increase caused by the surcharge load so as to determine the increases in the reinforcement forces for the internal stability calculations.

According to the FHWA design guideline, which is compatible to AASHTO (1996) Specifications, the reinforcement force T_i at i^{th} level is computed based on the lateral pressure $\sigma_{\text{H},i}$ and the tributary area A_i as given in Eq. (1).

$$\sigma_{\text{H},i} = K(\gamma z_i + \Delta\sigma_{\text{V},i}) + \Delta\sigma_{\text{h},i} \tag{1}$$

where K is the lateral earth pressure coefficient, $\Delta\sigma_{\text{V},i}$ is the increment of vertical stress due to the concentrated vertical surcharge assuming a 2V:1H pyramid distribution (Fig. 1), $\Delta\sigma_{\text{h},i}$ is the incremental horizontal stress due to the horizontal loads, and γz_i is the vertical stress at i^{th} level due to the overburden pressure. The calculation model for $\Delta\sigma_{\text{V},i}$, the 2V:1H pyramid distribution, however, is rather empirical and needs to be further refined.

Other relevant design recommendations by the FHWA design guideline when using GRS walls as bridge abutments include:

- Tolerable angular distortions between abutments or between piers and abutments of 0.005 for simple spans and 0.004 for continuous spans when bridge abutments are directly supported on the reinforced backfill.
- A minimum offset from the front of the facing to the centerline of bridge bearings of 1 m.
- A clear distance of 150 mm between the back face of the facing panels and the front edge of footing.
- Placement of the abutment footing on a bed of compacted coarse aggregate of 1 m thick when significant frost penetration is anticipated.
- Allowable bearing pressure of the reinforced backfill of 200 kPa.

Table 1
Summary of load application process

Step	Incremental load (kN)	Cumulative load (kN)	% Of total load	Loading description
1	78	78	22.4	Placement of PC box
2	69	147	42.2	First pouring of Remicon of 3 m^3
3	69	216	62.1	Second Remicon of 3 m^3
4	92	308	88.5	Third Remicon of 4 m^3
5	40	348	100.0	Add steel frame

It should be noted that most of the above recommendations are rather based on experiences with MSE wall abutment construction in which inextensible reinforcements were adopted, further studies on GRS abutment are warranted to establish sound basis for above recommendations.

3. Test wall description

The test wall was originally constructed in 2002 in order to investigate the short- and long-term performance of a two-tier GR-SRW. The measured performance during construction based on extensive field instrumentation has been reported by Yoo and Jung (2004). A brief discussion on the wall design and construction is given in this section.

The geometry of the test wall is shown in Fig. 2. The two-tier wall had an exposed height (H) of 5 m with the lower and upper tier height of 3.4 and 2.2 m, respectively. The wall was constructed to have no pre-batter angle with an offset distance between the upper and lower tiers of 1.0 m. As shown, 10 layers of PET reinforcement, having a rupture strength of 55 kN/m at strain of 12.5% with an average axial stiffness of $J = 700$ kN/m, were placed at a maximum vertical spacing of 0.6 m. For each tier, the reinforcement length ratio with respect to the respective tier height was kept constant at 1.0. The facing blocks, having a compressive strength of 21 MPa, were 450×330 mm in plan $\times$ 200 mm in height. Note that no provision was made for any future surcharge load in terms of the reinforcement distribution at the time of wall construction.

The backfill was a non-plastic well-graded silty sand, commonly known as weathered granite soil in Korea, classified as SW-SM soil as per ASTM 2487 (ASTM, 1992). The soil was compacted to 95% of its maximum unit weight (20 kN/m^3) to create the reinforced as well as retained zones. The estimated internal friction angle (ϕ') using a series of consolidated-undrained (CU) triaxial compression tests with pore pressure measurements and large scale direct shear tests at a density corresponding to the as-compacted state was approximately 35–37° with a shear stress intercept of 5–10 kPa. As-built design satisfied both the NCMA and FHWA design guidelines as given in Yoo and Jung (2004). Details of the wall construction can be found in Yoo and Jung (2004).

4. Full-scale load test

4.1. Test setup

The load test was carried out on August 2006, 4 years after the completion of wall construction. A gravity-type load was applied at the top of the wall using a precast concrete (PC) box frame, having dimensions of 2.4 m $\times$ 2.4 m in plan and 2.4 m in height, together with ready mixed concrete and a steel frame (Fig. 3). Placed on the top surface of the reinforced zone prior to the placement of the PC box was a concrete footing, having the same dimension of the PC box. The footing clear distance, measured from the back face of the upper tier-facing block, was approximately 0.2 m with the footing center aligned with the centerline of the test wall.

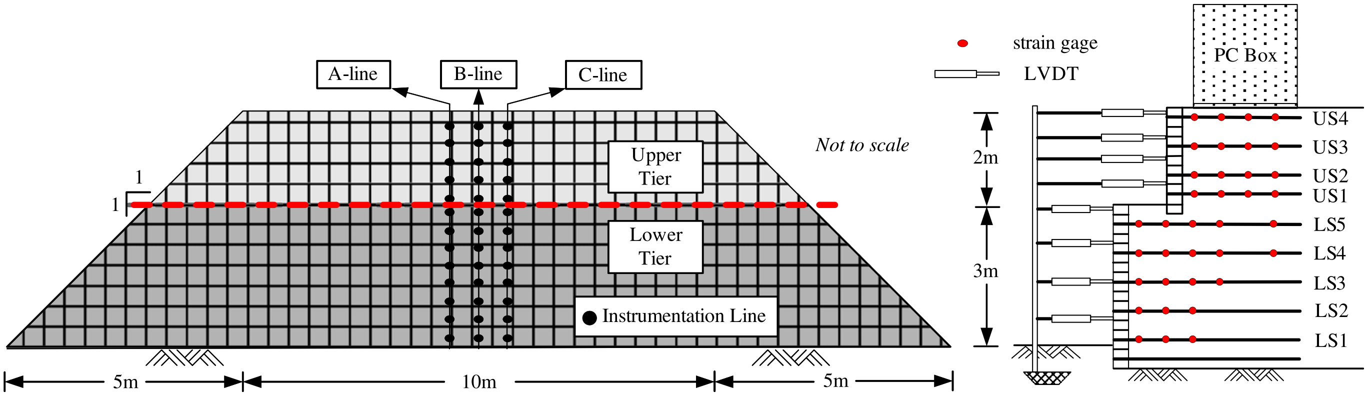

Fig. 4. Instrumentation layout.

A total of 348 kN of vertical load was applied on the footing, exerting 62 kPa to the top surface of the reinforced zone. The test load was applied in increments by controlling the volume of the ready mixed concrete poured into the PC box as summarized in Table 1. Each load increment was maintained for a sufficient amount of time to allow the stress to be transferred to the entire reinforced soil mass. The time for placement of a next load increment was decided based on the wall facing displacements measurements. A total of 5 h, 30 min were required to complete the test. The vertical pressure level of 62 kPa corresponded to one-third of the allowable bearing pressure specified by the FHWA design guideline, and therefore the test condition can be considered to be a working stress (i.e., serviceability) condition that is of most interest to designers.

4.2. Instrumentation

The performance of the test wall under the surcharge load was evaluated in terms of the wall facing displacements and the reinforcement strains. The layout of instrumentation program is shown in Fig. 4. Horizontal displacements of the wall facing were measured by using eight LVDTs having gauge length of 100 mm placed at locations along a vertical row as shown in Fig. 4. For redundancy optical leveling using a 3D total station (MONMOS Model NEA2A) was also carried out.

The surcharge load-induced reinforcement strains were measured using high-elongation strain gauges, manufactured by Tokyo Sokki Kenyujo Company (Model YFLA-5-1L). Note that these strain gauges were installed during the wall construction. They were mounted directly onto the selected reinforcement layers in three arrays, each 1 m apart laterally. Note that approximately 70% of 108 strain gauges had survived at the time of the load test. Table 2 summarizes the details of the instrumentation. More detailed information on the instrumentation program can be found in Yoo and Jung (2004).

Table 2
Details on instrumentation

Array/instrumentation	Location
Array A, B, C	−1.0, 0, +1.0 m From wall centerline
Optical survey target on wall facing column	0.1, 1.5, 0.9, 1.3, 1.7, 2.1, 2.5, 2.9 3.1, 3.5, 3.9, 4.3, 4.7 m Above wall base
Strain gauge	0.5, 1.0, 1.5 m Behind wall facing (LS1–LS3)
	0.5, 1.0, 1.5, 2.5 m Behind wall facing (LS4–LS5)
	0.5, 1.0, 1.5, 2.5, 3.0 m Behind wall facing (US1–US4)

4.3. Measured results

4.3.1. Horizontal wall displacement

Fig. 5 shows the progressive development of wall displacements along the height of the wall measured using the LVDTs. Also shown in this figure are the surcharge load levels during the loading steps. As seen in these figures, the stepwise increase in the lateral wall displacements is evident due to the stepwise increase in the surcharge load, showing a maximum displacement of 1.7 mm recorded at the top of the upper tier (U4) with displacements less than 0.5 mm in the lower tier. Of interest trend shown in Fig. 5 is that the

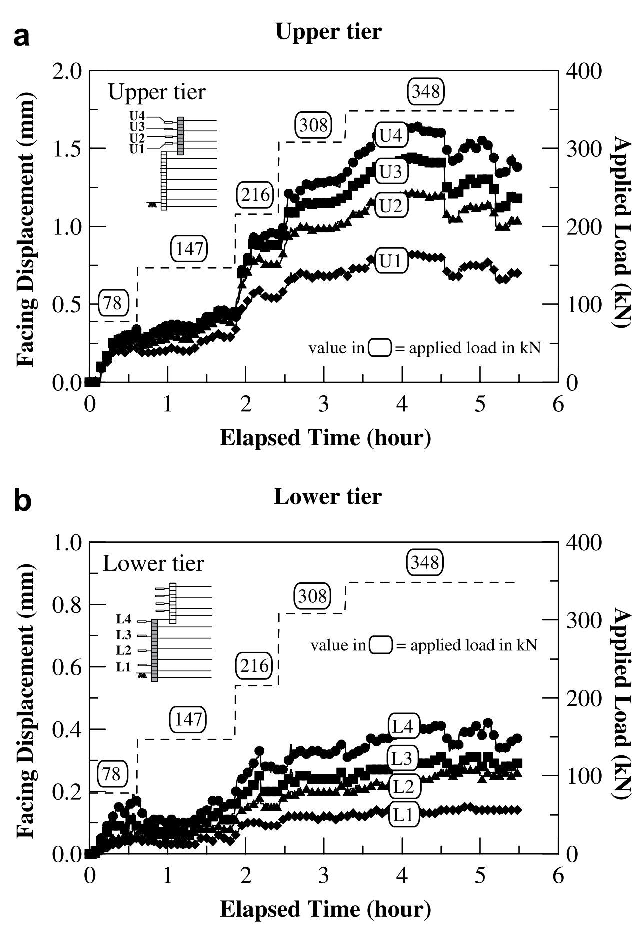

Fig. 5. Progressive development of wall displacements at monitoring points.

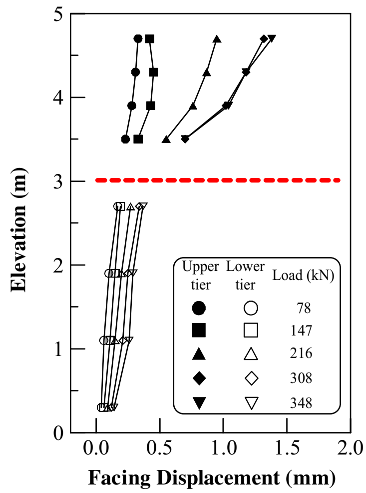

Fig. 6. Facing displacement profiles at various loading stages.

wall facing displacements tended to gradually develop over time immediately after the placement of each surcharge load, showing a tendency of the time dependent displacement, although not significant.

The horizontal wall facing displacement profiles at different loading stages are shown in Fig. 6. As seen, a cantilever-type wall movement pattern prevails both in the upper and the lower tiers with such a pattern being more pronounced in the upper tier. Also observed is the horizontal displacement at the bottom portion of the upper tier, as great as 50% of the maximum displacement at the top, or 0.7 mm, due to the horizontal displacement at the top of the lower tier.

As presented, the surcharge load of 348 kN, or 62 kPa, induced a maximum horizontal wall displacement less than 2 mm although no provision was made for the surcharge load during the wall design. The magnitudes of the measured wall displacements are in fact smaller than reported in the literature (Wu et al., 2006a) concerning load tests on GRS walls at a similar load level, although a direct comparison is not possible. No visible bulging on the wall facing in the vicinity of the loaded area was evident, demonstrating an excellent load carrying capacity of the test wall.

4.3.2. Reinforcement strains

The progressive development of the surcharge load-induced reinforcement strains is shown in Fig. 7 for selected layers. Also shown in Fig. 8 are the reinforcement strain distributions for the upper tier. No appreciable strains in the layers LS1–LS4 in the lower tier were recorded and therefore are not given here. The influence depth of the surface load is therefore thought to be slightly larger than the upper tier height of 2 m for the test condition.

In the upper layers, as seen in Fig. 7(a)–(c), the stepwise increases in strains due to the stepwise increase in the surcharge load are apparent with the maximum strain of 0.1% occurring at the top layer US4. In the lower tier as shown in Fig. 7(d), on the other hand, a maximum strain of 0.05% was recorded at the final load of 348 kN at the location 1.5 m away from the wall facing with essentially negligible strains elsewhere. A decrease in strain of approximately 0.08% is noticed at the mid location of the layer LS5, although the cause for such a trend is not immediately clear. Of interest trend shown in this figure is the development of the strain over time for a given load increment. For example, each load increment caused a sharp increase immediately after the load application, followed by a gradual decrease leading to a certain value. Such a trend is in fact similar to the observation in a series of plane strain compression tests (Kongkitkul et al., 2004; Yoo et al., 2005) and sustained

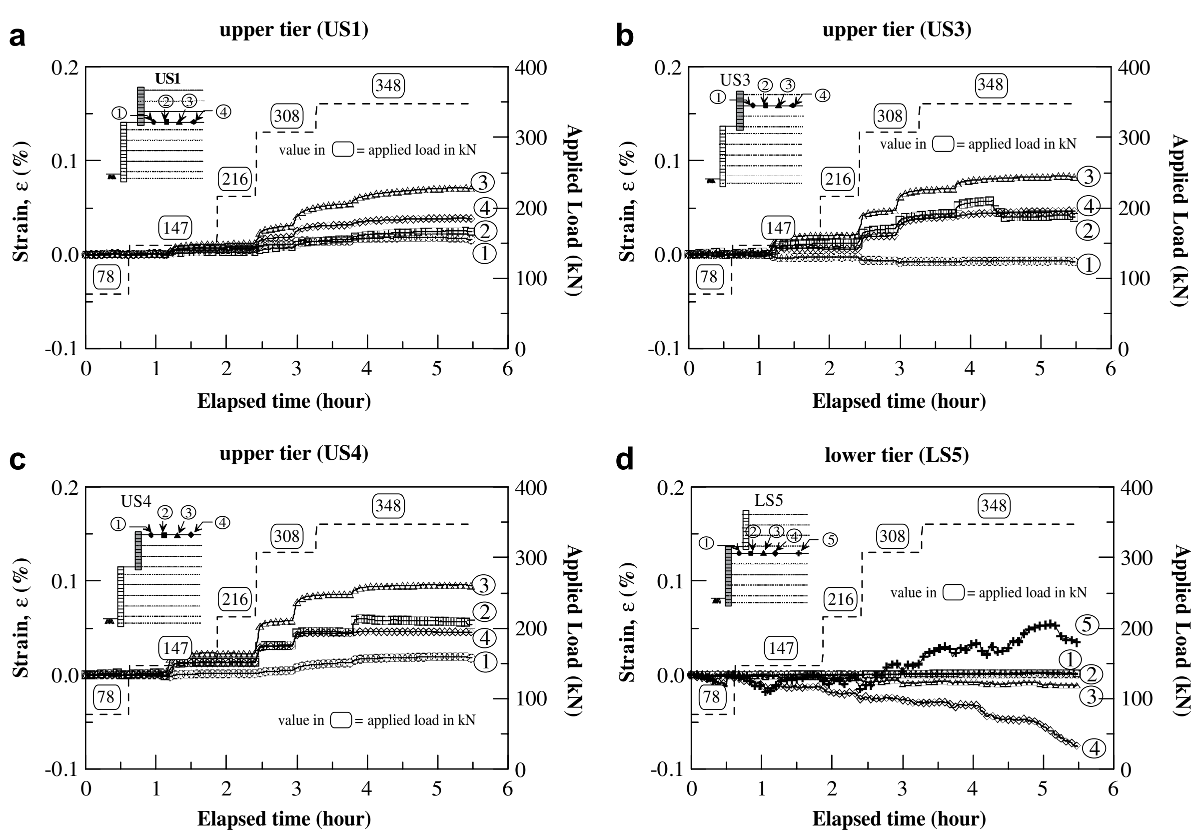

Fig. 7. Progressive development of reinforcement strains.

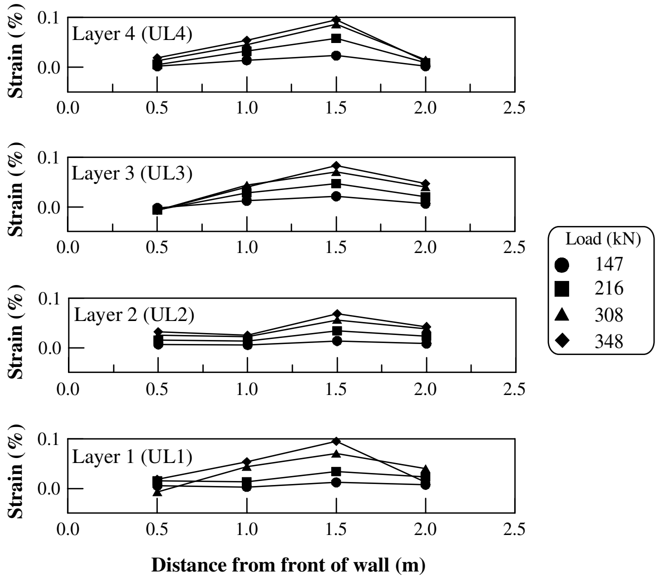

Fig. 8. Reinforcement strain distributions for upper tier at final loading stage.

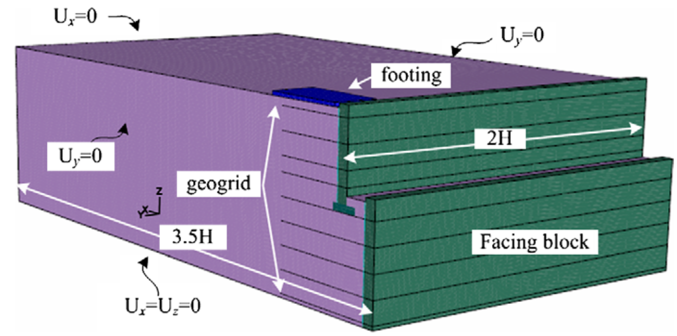

Fig. 9. Schematic view of finite element model.

loading tests on reduced-scale geosynthetic reinforced walls (Hirakawa et al., 2004; Yoo et al., 2005, 2007). Fig. 8 shows the surcharge load-induced reinforcement strain distributions for the upper tier layers. As seen, for each layer the maximum strain developed at some distance away, i.e., 1.5 m, from the wall facing.

The maximum measured strain of 0.1% would in fact yield an incremental reinforcement force ΔT less than 1 kN/m when inferred in conjunction with the results of in-isolation wide width tensile test conducted on the reinforcement, shown in Fig. 12 (to be shown later). Such a level of inferred reinforcement force ΔT is only a fraction of the calculated value of 8.3 kN/m according to the FHWA guideline, suggesting some degree of conservatism in the calculation model. A further study is necessary in this area to further refine the calculation model adopted in the FHWA design guideline.

In short, the surcharge load of 348 kN on a 2.4 m $\times$ 2.4 m loaded area induced a maximum reinforcement strain of 0.1% in the top most layer, while negligible reinforcement strains were developed in the rest of the layers in the lower tier. Considering that these surcharge load-induced strains are insignificant, it can therefore be concluded that the surcharge load did not impose any threat to the internal stability of the test wall even though the wall was not designed for the load, demonstrating an excellent load carrying capacity of the test wall.

5. Three-dimensional finite element analysis

A three-dimensional finite element analysis was additionally carried out on the test wall to further investigate the wall performance under a surcharge load well in excess of the test load. The 3D model was first calibrated against the load test data, to a limited extent, before deploying for analysis. The results were then used to examine the load carrying capacity and the relevant performance of the test wall under the surcharge load. Details of the 3D finite element modeling and the results are given in this chapter.

5.1. 3D finite element model

A commercial finite element code ABAQUS (2006) was used for analysis. ABAQUS was used in this study due to its robustness in numerical solution strategy for soil nonlinearity and the ability to simulate the sequential construction procedure of GR-SRWs. A 3D model was adopted rather than a 2D model in this study as this study was specifically focused on the surcharge loading situation similar to the test wall, i.e., a GR-SRW loaded by an isolated footing, which cannot be realistically simulated with a 2D model.

On account of the symmetry about the center of the footing, only half of the test wall was considered in the 3D modeling as shown in Fig. 9. The geometry of the test wall was rather simplified by adopting a model with dimensions having the width (y-direction) and the depth (x-direction) of 2H and 3.5H, respectively. In terms of the boundary condition, vertical rollers were placed at the boundaries perpendicular to x- and y-directions so that $U_x = U_y = 0$, as shown in Fig. 9. A fixed boundary condition in both horizontal and vertical directions was used at the foundation level as the wall was situated on a rather competent foundation.

Fig. 10 shows the 3D finite element mesh, consisting of 79,740 nodes and 20,802 elements, adopted in the analysis. The wall facing, the reinforced and retained soil zones were discretized using 20-node brick elements (C3D20R) with reduced integration, while the reinforcement was modeled using eight-node membrane elements (M3D8). The membrane elements are surface elements that transmit in-plane forces only (no moments) and have no bending stiffness and are particularly useful in modeling geosynthetic reinforcements as they can represent thin stiffening components in solid structures such as a reinforcing layer in a continuum.

The interface behavior between the wall facing and the backfill soil was modeled using a layer of thin elements having a relatively small shear modulus of $G = 0.5$ MPa with a large bulk modulus of $K = 10$ MPa to permit relative movement between the two media assuming an elastic behavior. Note that these properties are equivalent to those of the reported block interface properties (Hatami and Bathurst, 2006; Yoo and Song, 2006). Although ABAQUS provides a surface-based interface modeling option using 'contact pair', the contact pair was not adopted in modeling the interface in this study as significant numerical instabilities were encountered when activating contact pairs during the block and fill placement. No interface was introduced between the soil and the reinforcements assuming no slip between the backfill and the reinforcements. This is justified since pullout tests on many soils show that slip occurs in the soil and not at the interface of the reinforcement, unless the confining stress is extremely small. The block–block interface was not explicitly modeled as the introduction of interface elements between the blocks has insignificant effect on the wall performance for the reported block interface properties (Hatami and Bathurst, 2006; Yoo and Song, 2006). The discrete nature of the modular block wall facing was, however, taken into consideration by adopting a reduced Young's modulus for the facing block unit. The representative Young's modulus for the pseudo continuum wall facing was in fact found during the model calibration process as will be shown later.

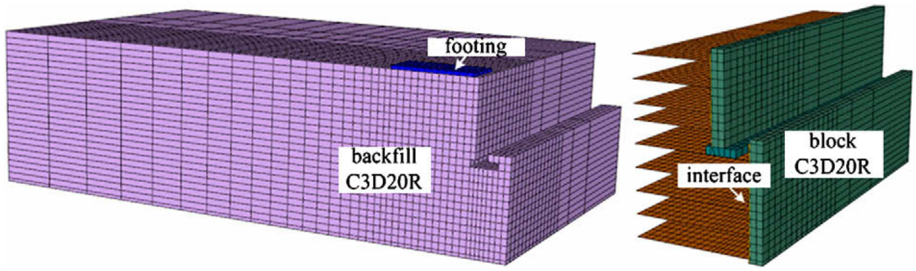

Fig. 10. 3D finite element mesh.

With regard to the constitutive modeling, the backfill soil was assumed to be an elasto-plastic material conforming to the modified Drucker–Prager/Cap failure criterion, while the facing block was assumed to behave in a linear elastic manner. The modified Drucker–Prager/Cap model is based on the addition of a cap yield surface to the Drucker–Prager plasticity model which provides an inelastic hardening mechanism to account for plastic compaction and helps to control volume dilatancy when the material yields in shear. In addition the hyperelastic material model available in ABAQUS was used to simulate the stress–strain behavior of the reinforcement. The hyperelastic material model is isotropic and nonlinear and is known to be valid for materials that exhibit the polymer-like material behavior. Details of the modified Drucker–Prager/Cap failure model and the hyperelastic model can be found in ABAQUS (2006).

Fig. 11 shows the simulated deviatoric stress vs. axial strain curves obtained from the modified Drucker–Prager/Cap model using the relevant model parameters given in Table 3 that were fitted to the CU test results for the specimens prepared as-compacted state. Note that the modified Drucker–Prager/Cap model parameters given in Table 3 are the best estimates taken from a literature by Helwany (2007) except d' and β' which were determined from the results of CU tests. As seen a reasonable agreement can be observed between the two sets of data. Presented in Fig. 12 are the results of the in-isolation constant rate of strain (CRS) of 10%/min according to the ASTM D4595 (ASTM, 1996) test protocol, fitted with the simulated results using the membrane elements together with the hyperelastic material model. Note that the results of the in-isolation CRS test were directly used as the material input for the hyperelastic material. As shown, a good agreement between the test results and the simulated results can be observed.

In simulating the load test, the step-by-step sequential bottom–up construction procedure was first simulated by adding facing blocks, 0.2 m thick soil layers, and the reinforcement layers at designated steps prior to the surcharge loading. Note that the addition of respective elements for soil layers and facing blocks automatically turned on their self-weights. Upon completion of the wall construction simulation, the surcharge load was then applied in increments.

5.2. Model calibration

The 3D model described above was calibrated using the results of the load test such as the surcharge load-induced horizontal wall facing displacements and the reinforcement strains. The model calibration was focused more or less on finding the equivalent Young's modulus of the wall facing as other properties of constituent components of the wall, such as the as-compacted backfill soil and the reinforcement, were reasonably well estimated from the extensive laboratory testing program at the time of the wall construction as discussed. A range of equivalent Young's modulus of the wall facing column $E_{w,eq}$, 1–10 GPa was considered, giving the equivalent wall flexural stiffness of per unit length of the wall, $(EI)_{w,eq}$ where I is the second moment of inertia, in the range of 3–70 MN$\cdot$m^2/m. The material properties of other wall components were kept constant.

The results of a series of analysis indicated that best matches between the measured and calculated data can be achieved when $(EI)_{w,eq} = 3$ MN$\cdot$m^2/m in terms of the wall facing displacements as shown in Fig. 13(a), in which the measured and numerically calculated displacements of the wall facing at the monitoring points at selected load levels are compared. As seen in Fig. 13(a), the general trends of the measured wall facing displacements are well captured in the numerical simulation for both the upper and lower tiers at the final load of 348 kN. A good agreement can also be seen in the predicted and the measured maximum strain profiles shown in Fig. 13(b). The measured strain distribution in the upper layers in Fig. 13(c), however, is not quite well captured by the numerical simulation, although the causes for such discrepancies are not immediately clear.

In short despite some discrepancies between the measured and the results form the 3D model; the 3D numerical model appears to be able to well capture the response of the test wall to

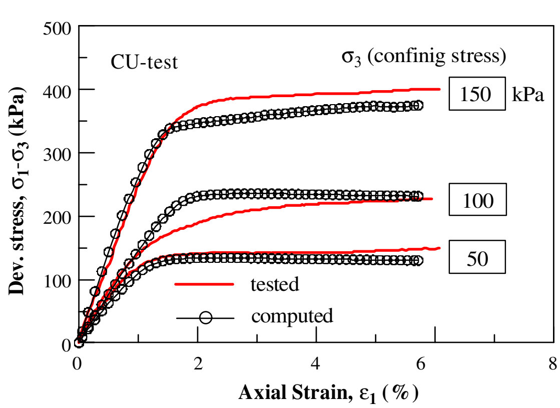

Fig. 11. Computed vs. measured CU test results.

Table 3
Modified Drucker–Prager/Cap model parameters for backfill soil

Material parameters	Backfill soil
Effective cohesion, d' (kPa)	20
Effective internal friction angle, β' (deg)	52
Eccentricity of cap yield surface, R	0.4
Constant for cap surface transition, α	0.05
Yield stress ratio, K	1.0
Young's modulus, E (MPa)	20
Unit weight, γ (kN/m^3)	19

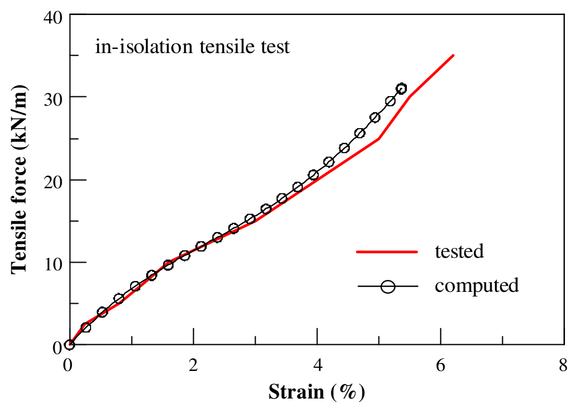

Fig. 12. Computed vs. measured in-isolation test of reinforcement.

the surcharge load. The equivalent flexural stiffness of the facing column of $(EI)_{w,eq} = 3\ \text{MN}\cdot\text{m}^2/\text{m}$ was therefore used in the subsequent 3D analysis with surcharge loads well in excess of the test load.

6. Predicted performance beyond working stress condition

6.1. General

The results of the 3D analysis for the test wall under a surcharge load well in excess of the test load are presented in this section in terms of the surcharge load-induced horizontal wall displacements and footing settlements, and reinforcement strains.

6.2. Footing settlement and wall deformation

Where fully supporting bridge loads, the settlement of abutment footing supporting the bridge beam is considered to be a key performance indicator and is required not to exceed 1% of the height of the load bearing wall (H) according to the existing maximum settlement criteria for bridge abutments (Wu et al., 2006a). The relationships between the applied surcharge pressure (q) and the footing settlement (S_v) are examined in Fig. 14. As shown, the q–S_v relationships tend to yield the ultimate load carrying capacity of the test wall approximately of 420 kPa with essentially no differential settlement of the footing during the entire loading stages,

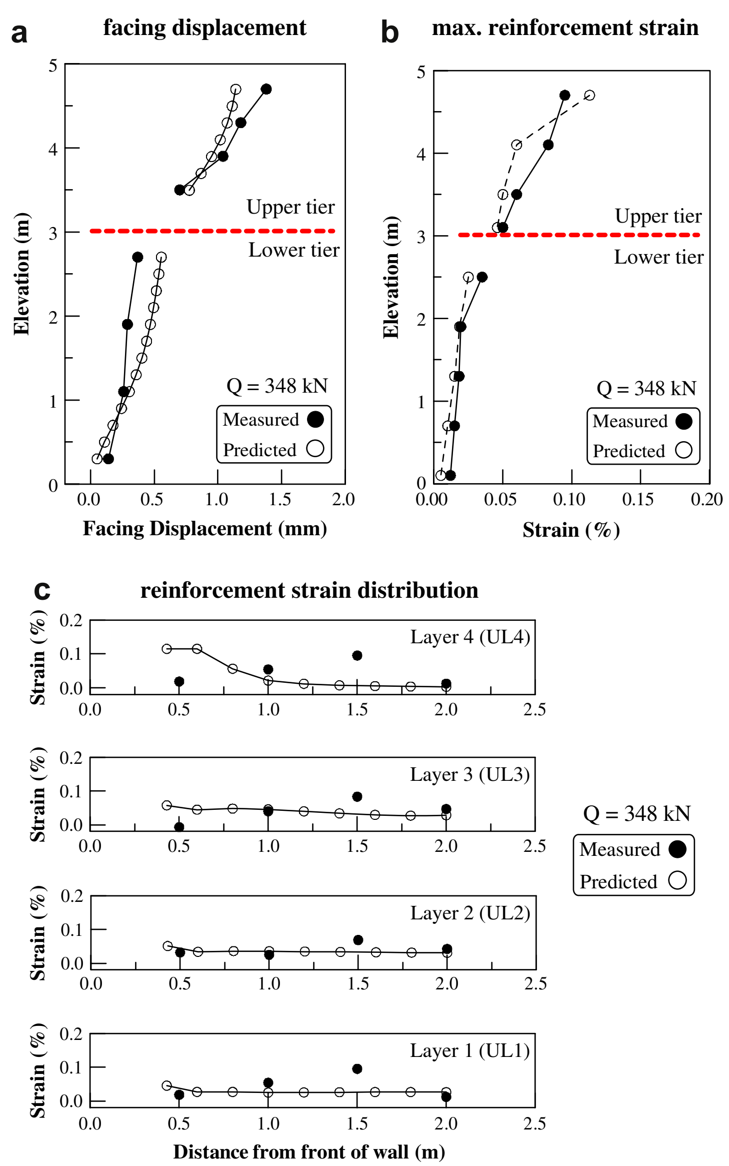

Fig. 13. Measured and predicted results ($(EI)_{w,eq} = 3\ \text{MN}\cdot\text{m}^2/\text{m}$).

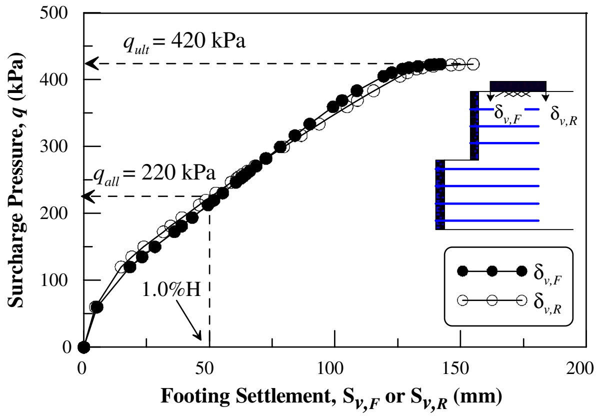

Fig. 14. Development of footing settlement with surcharge pressure.

suggesting that the footing distortion is not of concern for GR-SRWs under a similar loading condition. Judging from the 1%*H* criterion the allowable bearing pressure for the wall is deemed in the neighborhood of 220 kPa, close to the allowable bearing pressure of 200 kPa specified in the FHWA design guideline.

The relationships between the applied surcharge pressure (q) and the maximum facing displacement (δ_h) are shown in Fig. 15 for both tiers. The q–δ_h curves show that δ_h nonlinearly increases with the surcharge pressure level up to 120 kPa after which δ_h almost linearly increases with q. Such a trend is similar in trend to the results from the previous studies based on full-scale load tests and numerical studies (Wu et al., 2006a,b). At the allowable bearing pressure of 200 kPa, the maximum wall displacements for the upper and lower tiers are approximately 5 mm. Even at the ultimate surcharge pressure level, i.e., $q = 420$ kPa, less than 12 mm of maximum wall displacements are induced in both tiers, demonstrating excellent load carrying capacity of the GR-SRW.

Fig. 16 shows the surcharge load-induced wall displacements at selected surcharge pressure levels up to 420 kPa. Note that the horizontal displacements are shown in these figures in terms of the horizontal displacements at the wall face ($\delta_{h,face}$) and those behind ($\delta_{h,ext}$) the reinforced soil block. The average horizontal displacement within the reinforced soil block $\delta_{h,int}$ can simply be obtained by subtracting $\delta_{h,ext}$ from $\delta_{h,face}$. As seen in the displacement profiles for the upper tier shown in Fig. 16(a), the horizontal facing displacement profiles tend to follow a translation type movement as q increases with a maximum displacement of approximately 25 mm occurring at $q = 420$ kPa. The horizontal displacements at the back of the reinforced soil block (i.e., external deformation) are

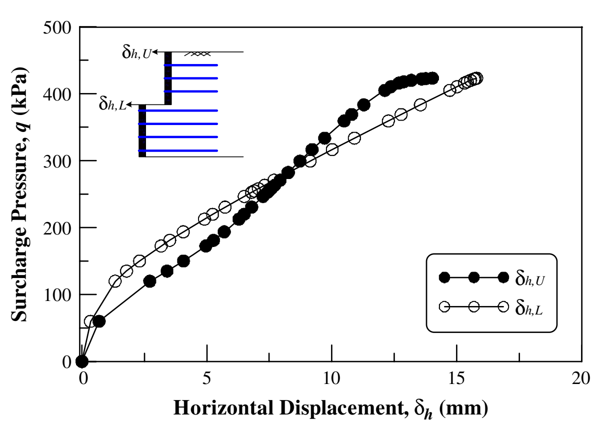

Fig. 15. Development of horizontal facing displacement with surcharge pressure.

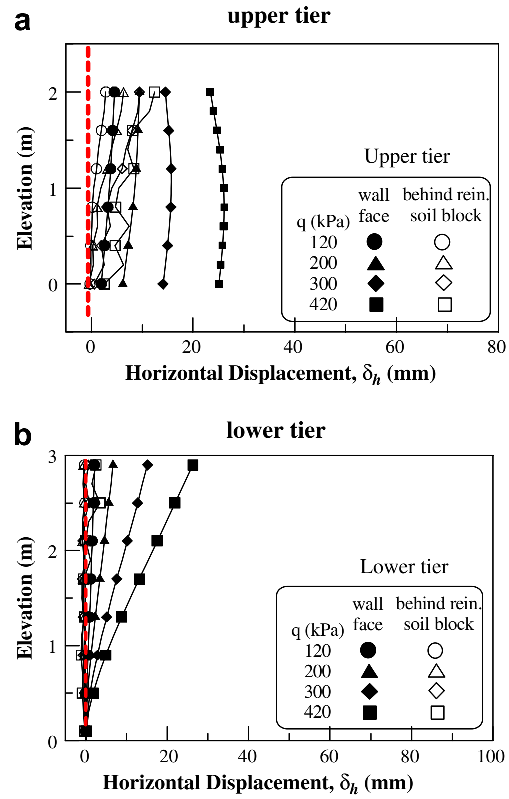

Fig. 16. Horizontal displacements of wall at various loading stages.

less than 10 mm, suggesting that the average horizontal displacements within the reinforced soil block are on the order of 15 mm. Such a trend implies that both the internal and external stabilities of the upper tier are affected by the surcharge load. For the lower tier in Fig. 16(b), however, a cantilever-type displacement pattern prevails in the facing displacement profiles with their maxima at the top throughout the entire loading stages showing a maximum displacement of 25 mm at $q = 420$ kPa. Unlike the upper tier the horizontal displacements at the back of the reinforced soil block, however, appear to be negligible, suggesting that the horizontal wall displacements due to the surcharge load are mainly associated with the internal deformation within the reinforced soil block, an indication that the surcharge loading is mainly relevant for the internal stability of the lower tier.

6.3. *Reinforcement strains*

The progressive development of the reinforcement strains (ε_g) with the surcharge pressure (q) is shown in Fig. 17. Note that the strains represent maximum incremental strains for the reinforcement layers. Similar to the horizontal wall facing displacements plot shown in Fig. 15, the q–ε_g relationships appear to be nonlinear up to the surcharge pressure of 120 kPa, after which ε_g tends to linearly increase with q until the surcharge pressure reaches its ultimate value of 420 kPa. The results in Fig. 17 are further examined in Fig. 18 in terms of the maximum strain profile at selected surcharge pressure levels up to $q = 420$ kPa. As expected, for a given surcharge load level the largest strain is developed in the upper most layer, below which a rapid decrease in strain is observed. At the surcharge pressure of 420 kPa, 1.5–4% of strains are developed in the reinforcement layers in the upper tier with less than 1.5% of strains being developed in the lower tier layers. Considering that the reinforcement strains directly proportional to the

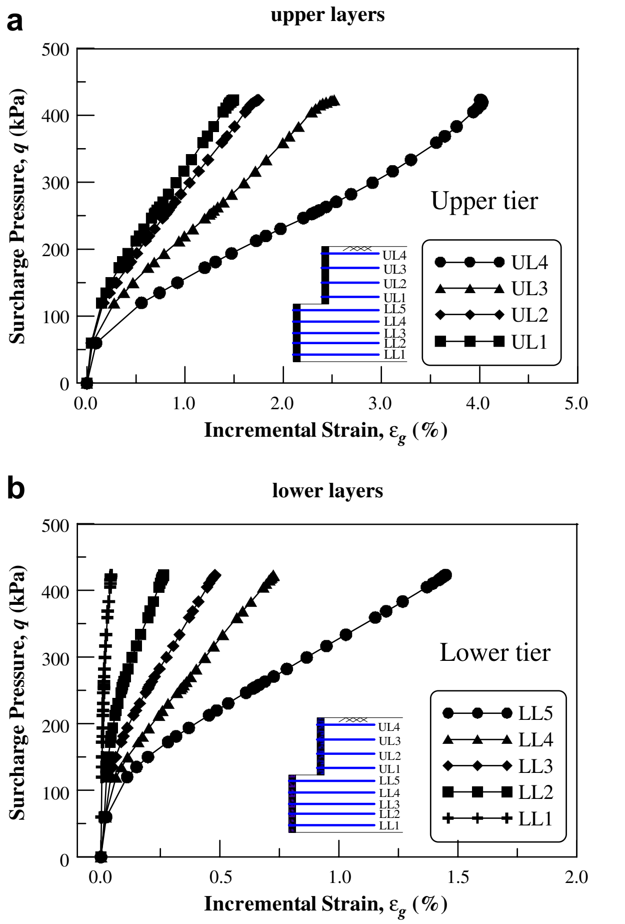

Fig. 17. Progressive development of incremental reinforcement strain at various loading stages.

horizontal stresses, such a trend in fact well agrees with the approach by the FHWA design guideline in which an exponential decrease in the surcharge load-induced stress with depth is assumed by adopting the 2V:1H approach. In addition, it can be seen that the allowable bearing pressure of 200 kPa only induces additional reinforcement strains less than 1.5%, imposing no threat to the internal stability of the wall, even with the reported construction-induced reinforcement strains of approximately 2% (Yoo and Jung, 2004).

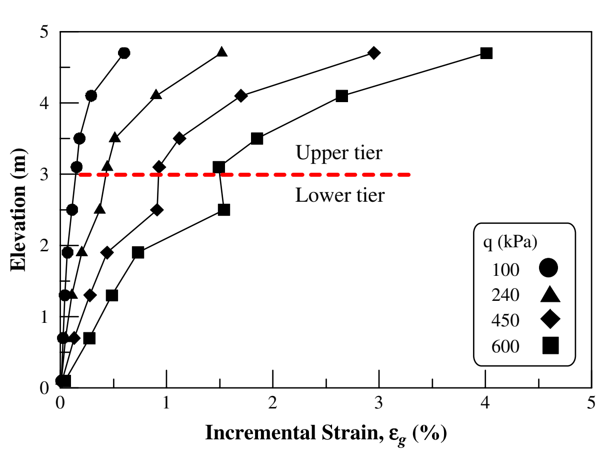

Fig. 18. Incremental reinforcement strain profiles at various loading stages.

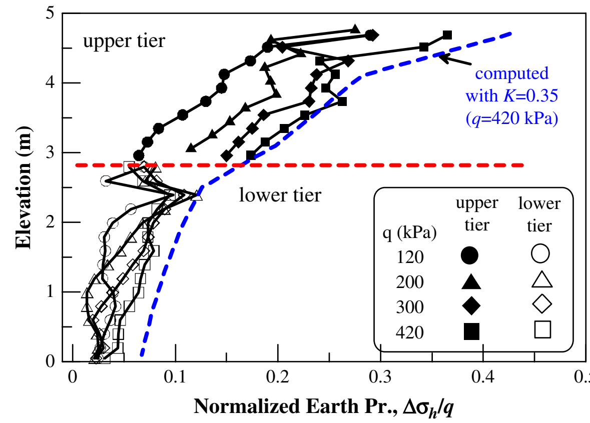

Fig. 19. Normalized incremental horizontal stress profiles.

The effect of the surcharge load on the internal stability of the wall is further investigated using the surcharge load-induced horizontal stresses ($\Delta\sigma_h$) acting at the back of the facing block in Fig. 19. Note that normalized horizontal stresses with respect to the applied pressure (q) are presented in this figure. Also shown in this figure are the results for $q = 420$ kPa computed by the FHWA method using the 2V:1H approach together with a lateral earth pressure coefficient of $K = 0.35$. As seen, the normalized horizontal stresses tend to increase with increasing q, implying that $\Delta\sigma_h/q$ is not constant but increases with the level of q. When $q = 420$ kPa, i.e., the ultimate state, $\Delta\sigma_h/q$ is largest, exhibiting a maximum of $(\Delta\sigma_h/q)_{max} = 0.35$, at the top of the upper tier, immediately below the footing, then sharply decreases with depth thereafter to $\Delta\sigma_h/q = 0.15$ at the bottom of the upper tier. In the lower tier, however, $\Delta\sigma_h/q$ profiles appear to be relatively uniform along the height at all levels of q with $\Delta\sigma_h/q = 0.05$–0.1. Again the horizontal stress distributions shown above also confirm that the 2V:1H approach adopted by the FHWA guideline is appropriate at least in qualitative terms.

Fig. 20 presents contour as well as vector plots for the strains in the top reinforcement layer U4, i.e., immediately below the surcharge load. The axial strains both in the directions perpendicular ($\varepsilon_{g,x}$) and parallel ($\varepsilon_{g,y}$) to the wall facing are shown. As shown in Fig. 20(a) and (b), larger strains are developed directly under the edge of the footing, suggesting that placement of an additional reinforcement layer directly under the footing edge is desirable if possible stress concentration in that zone is to be avoided. Also shown is that the strains in the direction parallel to the wall facing, i.e., $\varepsilon_{g,y}$, under the edge of the footing are approximately one-third of the maximum strain in the direction perpendicular to the wall facing, $\varepsilon_{g,x}$. Considering the current practice that overlapping parts of each roll of reinforcement are typically nailed with "U" staples through its aperture into the backfill, the overlapping part should be designed to have at least one-third of the tensile resistance in the machine direction. In addition, as illustrated in Fig. 20(c), the surcharge load results in a principal strain rotation, especially in the front edge of the footing, implying that the tensile resistance of the reinforcement against biaxial or oblique loading may be an important issue when a large surcharge load is applied as a form of an isolated footing load. Such a trend cannot be well captured in an approximated 2D plane strain modeling for loading conditions similar to the one considered in this study. The issue of 2D modeling of a 3D loading condition is not the scope of this paper and will not be discussed further.

The surcharge load-induced reinforcement strains are depicted in Fig. 21 from which the influence zone for the surcharge load can be inferred. As shown at the applied pressure of 420 kPa, the

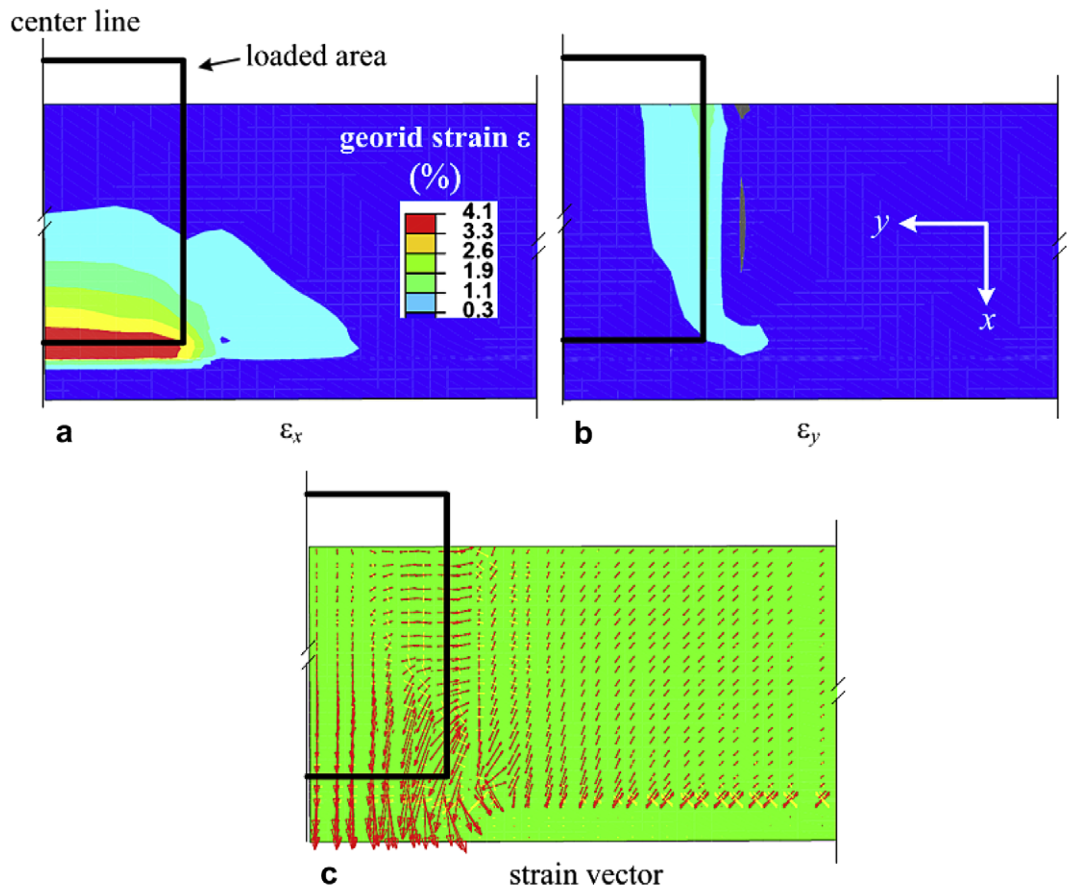

Fig. 20. Incremental strain plots for layer U4 ($q = 420$ Pa).

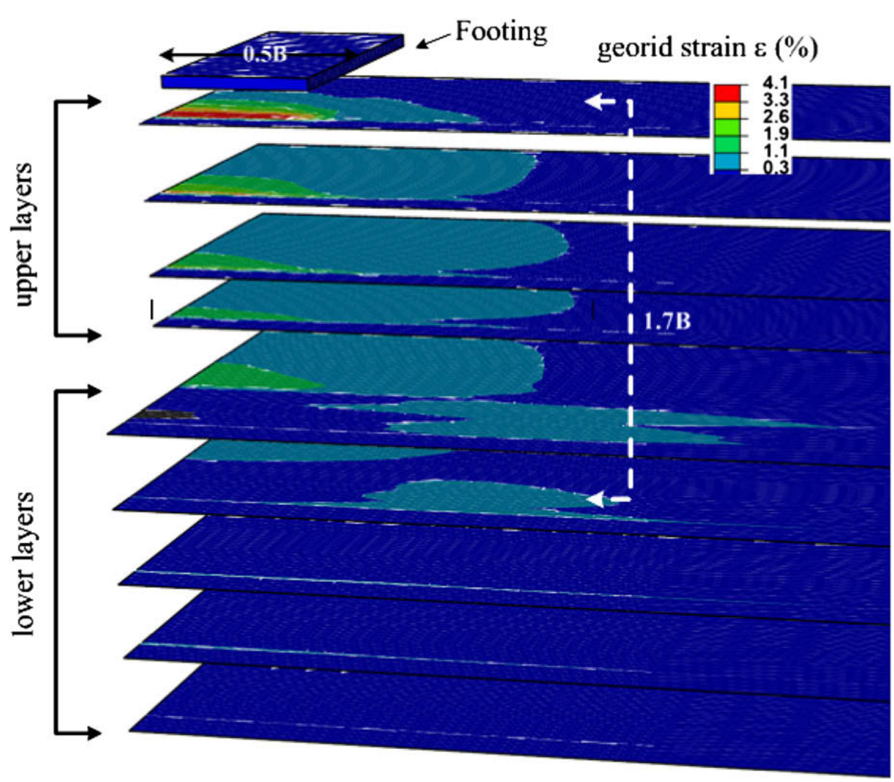

Fig. 21. Zone of strain increase for upper tier reinforcement layers ($q = 420$ Pa).

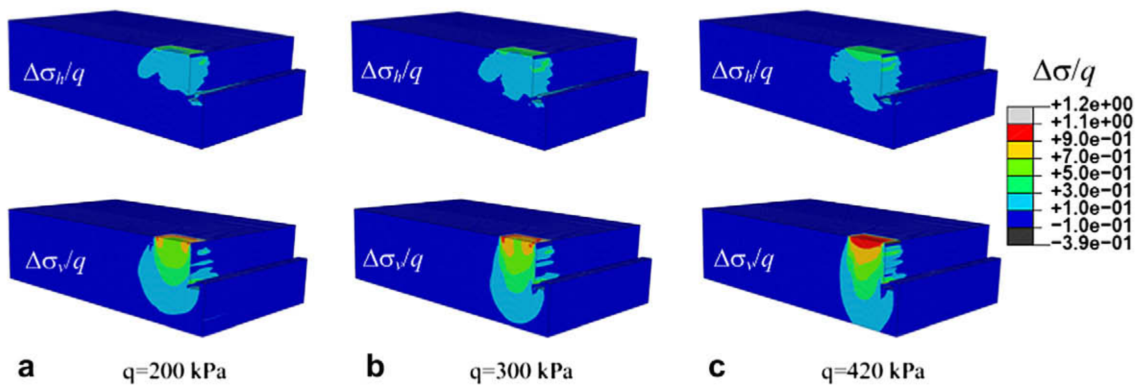

Fig. 22. Contour plots for normalized incremental horizontal and vertical stresses at various loading stages.

reinforcement strain increase is confined within the upper tier layers and the top two layers of the lower tier. Such a trend is in good agreement with the contour plots of the normalized incremental stresses $\Delta\sigma/q$ at selected load levels shown in Fig. 22. For example, the incremental horizontal stresses $\Delta\sigma_h/q$ are confined within the upper tier although the incremental vertical stresses $\Delta\sigma_v/q$ tend to extend to the full depth of the wall. The extent to which the surcharge load induces stresses appears to vary with the type of stress, i.e., $\Delta\sigma_v$ or $\Delta\sigma_h$. A further study is, however, warranted for walls with different geometries and surcharge loading conditions other than those considered in this study if the influence zones for various conditions are to be defined.

7. Conclusions

This paper presents the results of a full-scale load test and a 3D finite element analysis on a two-tier, 5 m high, geosynthetic reinforced segmental retaining wall subjected to a surcharge load. The load test was carried out aiming at getting insight into the performance of the wall under a working load and furnishing a complete set of data for calibration of the 3D finite element model. The calibrated 3D finite element model was used to investigate the wall behavior under a surcharge load well in excess of the test load. The following conclusions can be made based on the finding of the current study.

(1) The measured results indicated that a surcharge pressure of 62 kPa caused wall displacements and reinforcement strains within serviceability limits showing maximum values of 1.5 mm and 0.1%, respectively, although the wall was not designed for the surcharge load. This demonstrates an excellent load carrying capacity of the test wall.
(2) The effect of the surcharge load was more pronounced on the upper tier than on the lower tier. The inferred reinforcement forces from the measured strains were significantly smaller than the calculated based on the FHWA design guideline.
(3) The predicted results using the 3D finite element model yielded the ultimate load carrying capacity and the allowable bearing pressure of the test wall approximately of 420 and 220 kPa, respectively. No sign of differential settlement of the footing was evident suggesting that the footing distortion is not of concern. The load carrying capacity of the wall performance was governed by the bearing capacity failure of the backfill soil rather than the rupture of the reinforcements.
(4) The surcharge load-induced reinforcement strains and the horizontal stresses behind the wall facing block showed an exponential decrease with depth, agreeing with the approach by the FHWA design guideline in which an exponential decrease in the surcharge load-induced stress with depth is assumed by adopting the 2V:1H approach.
(5) The reinforcement strain vector plot indicated an evidence of a principal strain rotation, demonstrating the importance of considering tensile resistance of reinforcement in biaxial or oblique loading for walls subjected to an isolated footing load.

Acknowledgement

This work was supported by Grant No. R01-2004-000-10953-0 from the Basic Research Program of the Korea Science & Engineering Foundation. The financial support is gratefully acknowledged. Special thanks go to my former students Mr. Hyuck-Sang Jung, Young-Hoon Kim, Dae-Hee Han, and Yosep Byun for conducting the load test and Ms. Ah-Ran Song for preparing the 3D finite element model.

References

AASHTO, 1996. Standard Specifications for Highway Bridges, with 2000 Interims, American Association of State Highway and Transportation Officials, fifteenth ed. Washington, D.C., USA, 686 p.
ABAQUS Inc., 2006. ABAQUS User's Manual, Version 6.7. Abaqus, Inc., Pawtucket, Providence, RI.
Adams, M., 1997. Performance of a prestrained geosynthetics reinforced soil bridge pier. In: Wu, J.T.H. (Ed.), Mechanically Stabilized Backfill. A.A. Balkema Publisher, Rotterdam, pp. 35–53.
Al Hattamleh, O., Muhunthan, B., 2006. Numerical procedures for deformation calculations in the reinforced soil walls. Geotextiles and Geomembranes 24 (1), 52–57.
ASTM, 1992. Standard test method for classification of soils for engineering purposes. ASTM D2487-90. In: Annual Books of ASTM Standards, vol. 4.08, West Conshohocken, PA, pp. 326–336.
ASTM, 1996. Standard test method for tensile properties of geotextiles by the wide-width strip method. ASTM D4595. In: Annual book of ASTM standards, vol. 4.09, West Conshohocken, PA, pp. 698–708.
Benigni, C., Bosco, G., Cazzuffi, D., Col, R.D., 1996. Construction, performance of an experimental larger scale wall reinforced with geosynthetics. In: Ochiai, H., Yasufuku, N., Omine, K. (Eds.), Earth Reinforcement, vol. 1. A.A. Balkema Publisher, Rotterdam, pp. 315–320.
Chen, R.H., Chiu, Y.M., 2008. Model tests of geocell retaining structures. Geotextiles and Geomembranes 26 (1), 56–57.
Chen, H.-T., Hung, W.-Y., Chang, C.-C., Chen, Y.-J., Lee, C.-J., 2007. Centrifuge modeling test of a geotextile-reinforced wall with a very wet clayey backfill. Geotextiles and Geomembranes 25 (6), 346–359.
FHWA, 2001. Mechanically Stabilized Earth Walls and Reinforced Soil Slopes, Design and Construction Guidelines. Federal Highway Administration Publication No. FHWA-NHI-00-043. US Department of Transportation, Washington, D.C., USA, 418 pp.
Gotteland, Ph., Gourc, J.P., Villard, P., 1997. Geosynthetics reinforced structures as bridge abutments: full scale experimentation and comparison with modelisations. In: Wu, J.T.H. (Ed.), Mechanically Stabilized Backfill. A.A. Balkema Publisher, Rotterdam, pp. 25–34.
Hatami, K., Bathurst, R., 2006. Numerical model for reinforced soil segmental walls under surcharge loading. Journal of Geotechnical and Geoenvironmental Engineering 132 (6), 673–684.
Helwany, S., 2007. Applied Soil Mechanics with ABAQUS® Applications. Wiley, New York.

Hirakawa, A., Uchimura, T., Shibata, Y., Tatsuoka, F., 2004. Deformation characteristics of geosynthetics retaining wall loaded on the crest. In: Shim, J.B., Yoo, C., Jeon, H.J. (Eds.), Proceedings of Third Asian Regional Conference On Geosynthetics, Seoul, Korea, pp. 240–247.

Ketchart, K., Wu, J.T.H., 1997. Performance of geosynthetic-reinforced soil bridge pier and abutment, Denver, Colorado, USA. In: Wu, J.T.H. (Ed.), Mechanically Stabilized Backfill. A.A. Balkema Publisher, Rotterdam, pp. 101–116.

Kongkitkul, W., Uchimura, T., Tatsuoka, F., 2004. Residual deformation due to the viscous property during cyclic loading of geosynthetic reinforcement. In: Shim, J.B., Yoo, C., Jeon, H.J. (Eds.), Proceedings of Third Asian Regional Conference On Geosynthetics, Seoul, Korea, pp. 988–995.

Lee, K.Z.Z., Wu, J.T.H., 2004. A synthesis of case histories on GRS bridge-supporting structures with flexible facing. Geotextiles and Geomembranes 22 (4), 181–204.

Leshchinsky, D., Han, J., 2004. Geosynthetic reinforced multitiered walls. Journal of Geotechnical and Geoenvironmental Engineering 130 (12), 1225–1235.

Miyata, K., Kawasaki, H., 1994. Reinforced soil retaining walls by FRP geogrid. In: Tatsuoka, F., Leshchinsky, D. (Eds.), Recent Cases Histories of Permanent Geosynthetics-reinforced Soil Retaining Wall. A.A. Balkema Publisher, Rotterdam, pp. 253–257.

NCMA, 1997. Design Manual for Segmental Retaining Walls, second ed. National Concrete Masonry Association, Herndon, Virginia, USA, 289 pp.

Nouri, H., Fakher, A., Jones, C.J.F.P., 2006. Development of horizontal slice method for seismic stability analysis of reinforced slopes and walls. Geotextiles and Geomembranes 24 (2), 175–187.

Werner, G., Resl, S., 1986. Stability mechanisms in geotextile reinforced earth-structures. In: III International Conference on Geotextiles, Vienna, Austria, vol. 4, pp. 1131–1135.

Won, M.-S., Kim, Y.-S., 2007. Internal deformation behavior of geosynthetic-reinforced soil walls. Geotextiles and Geomembranes 25 (6), 10–22.

Wu, J.T.H., Ketchart, K., Adams, M., 2001. GRS Bridge Piers and Abutments. Report FHWA-RD-00-038. FHWA, US Department of Transportation, 136 pp.

Wu, J.T.H., Lee, K.Z.Z., Helwany, S.B., Ketchart, K., 2006a. Design and Construction Guidelines for GRS Bridge Abutments with a Flexible Facing. Report 556. National Cooperative Highway Research Program, Washington, D.C., 132 pp.

Wu, J.T.H., Lee, Z.Z., Pham, T., 2006b. Allowable bearing pressures of bridge sills on GRS abutments with flexible facing. Journal of Geotechnical and Geoenvironmental Engineering 132 (7), 830–841.

Yoo, C.S., Kim, J.S., 2002. Effect of foundation stiffness on behavior of soil-reinforced segmental retaining walls. Journal of Korean Geotechnical Society 18 (8), 7–19.

Yoo, C., Jung, H.S., 2004. Measured behavior of a geosynthetic-reinforced segmental retaining wall in a tiered configuration. Geotextiles and Geomembranes 22 (5), 359–376.

Yoo, C., Kim, S.B., Lee, B.W., 2005. Time-dependent deformation characteristics of geosynthetics-reinforced soil using plane strain compression tests. Korean Journal of Geotechnical Engineering 21 (10), 85–97. Korean Geotechnical Society.

Yoo, C., Song, A.R., 2006. Effect of foundation yielding on performance of two-tier geosynthetic reinforced segmental retaining walls – a numerical investigation. Geosynthetics International 20 (3), 110–120.

Yoo, C., Kim, S.B., Kim, Y.H., Han, D.H., 2007. Time-dependent deformation characteristics of geosynthetic reinforced modular block walls under sustained/cyclic loading. Korean Journal of Geotechnical Engineering 23 (6), 1–17. Korean Geotechnical Society.